Sample Solutions to HW3

26.April.2024

Q1 Understand the Lifshitz Theory of vdW Interactions

1. Temperature-dependency of interaction energy

   Within a small frequency range $\delta\nu = \nu_{\text{low}} - \nu_{\text{high}}$, the number of frequencies points δn is approximately: $\delta n = h\delta\nu/(2\pi k_{\text{B}}T)$. Therefore the contributions to the Hamaker constant within this frequency range is:

   $$\frac{3k_{\text{B}}T}{2}\sum_{\nu_n\geq\nu_{\text{low}}}^{\nu_n\leq\nu_{\text{high}}}\Delta_{13}(i\nu_n)\Delta_{23}(i\nu_n) \approx \frac{3k_{\text{B}}T}{2}\cdot\delta n\cdot\Delta_{13}\Delta_{23} \approx \frac{3h\delta\nu}{4\pi^2}\cdot\Delta_{13}\Delta_{23} \tag{1}$$

   If Δ_{13} and Δ_{23} do not change within $\delta\nu$, the results in Eq. 1 can be regarded as independent of T.

2. Model $\varepsilon(i\nu)$

   Based on the single-oscillator Lorentz model, the zero-frequency $\varepsilon = 1 + f_{\text{osc}} = n^2$, which leads to $f_{\text{osc}} = 1.34$. The $\varepsilon(i\nu)$ of such material is seen to be monotonically decaying with ν (Figure 1).

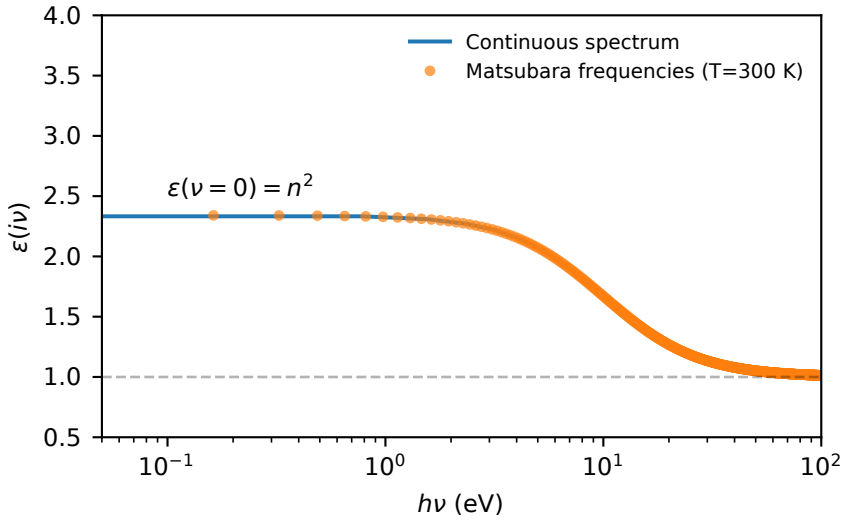

Figure 1: Frequency-dependent $\varepsilon(i\nu)$ in the single-oscillator Lorentz model.

3. T-dependency of Hamaker constant

   The dependency of Hamaker constant of A_{a} with T is shown in Figure 2. As expected, the Hamaker constant almost does not depend on the temperature when $T < 10^4$, indicating the assumption used in (1) is quite reasonable. In other words, even if the London dispersion theory is developed at 0 K, the results do not change at room temperature.

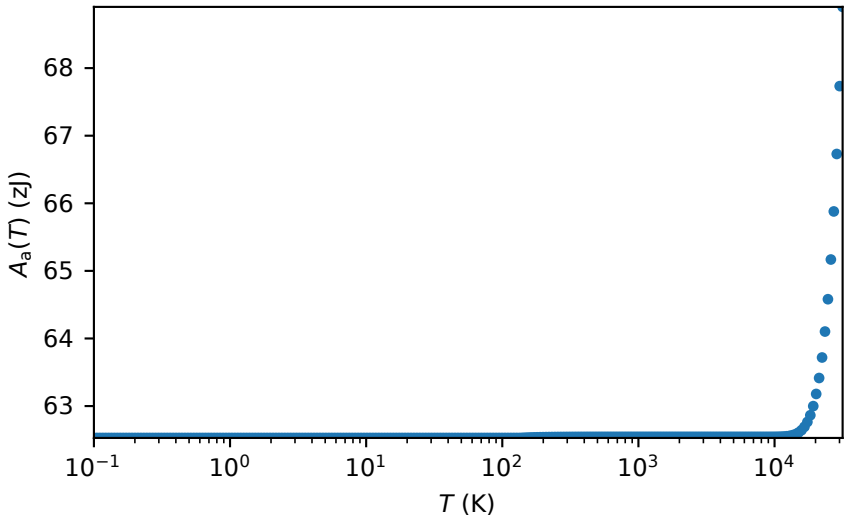

Figure 2: Temperature-dependent A_{a} (in zepto-Joule) using the single-oscillator Lorentz model.

4. Convert experimental spectra to $\varepsilon(i\nu)$

   The values of $\varepsilon(i\nu)$ of different materials can be seen in Figure 3. Within low frequency range $h\nu < 4$ eV, we have $\varepsilon_{\mathrm{SiO_2}} < \varepsilon_{\mathrm{BrPh}} < \varepsilon_{\mathrm{Au}}$.

5. Calculation of A_{132}

   The A_{132} of the SiO_2-BrPh-Au system is calculated to be 22.3 zJ. This is because the attractive contributions at higher energy range (red region in Figure 4) dominates over the repulsive contributions (blue region in Figure 4).

6. Conditions of retardation effect

   The condition of retardation effect is:

$$\begin{aligned} \tau \cdot \omega &\gg 1 \\ \frac{2d}{c}\omega &\gg 1 \\ d \cdot (\hbar\omega) &\gg \frac{\hbar c}{2} \end{aligned} \tag{2}$$

   where $\hbar c/2 = 98.7$ nm·eV. Therefore, we can conclude the retardation effect is only significant for case (d), that $h\nu = 50$ eV and $d = 50$ nm. Note here we ignore the impact of ε on the speed of light.

   A general rule is that the retardation effect is significant for longer separation d and higher frequency ω (or ν). It is natural to think if we introduce the retardation effect, the low-frequency repulsive contribution in (5) can be more prominent.

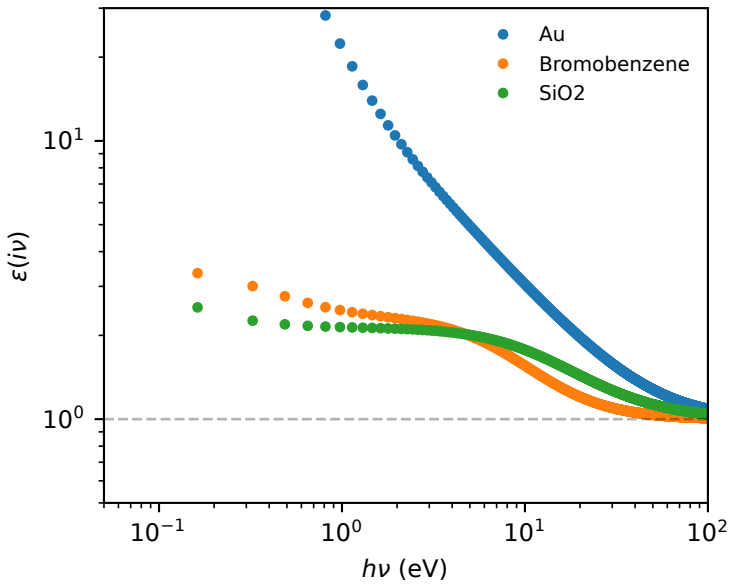

Figure 3: Comparison between $\varepsilon(i\nu)$ of SiO_2, Bromobenzene and gold using the Kramers-Kronig relations. The data points are Matsubara frequencies at $T = 300$ K.

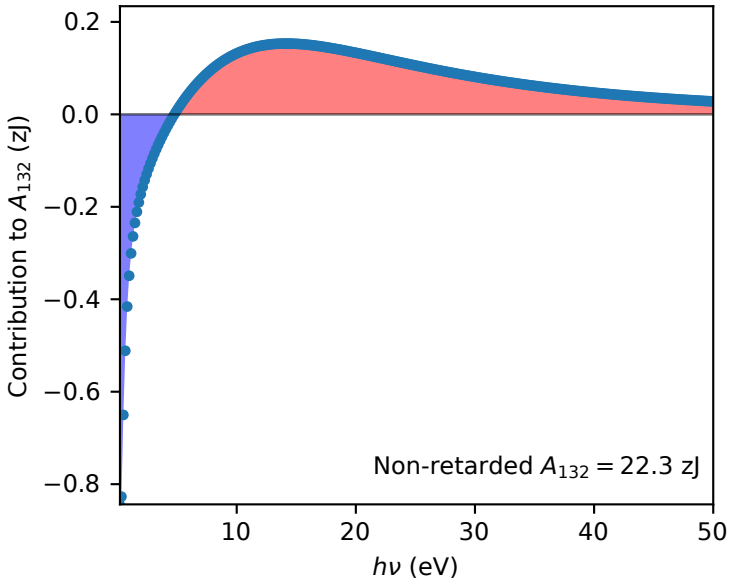

Figure 4: Frequency-dependent contributions to the Hamaker constant A_{132} of the SiO_2-BrPh-Au system. The Hamaker constant is still positive since the attractive contributions ($h\nu > 5$ eV) is dominating over the repulsive contributions ($h\nu < 5$ eV)

7. Repulsive interaction in retarded regime.

   The pressure $F_{132}(d)$ as function of d (Figure 5).

   To make illustration more appealing, we plot the $F_{123}(d)$ only for $d > 15$ nm. A repulsive pressure exists for separation larger than 20 nm. This allows the repulsive force measurable at the distance of 20 - 50 nm using atomic force microscopy (AFM), see Munday et al. *Nature* **457**, 170–173 (2009). .

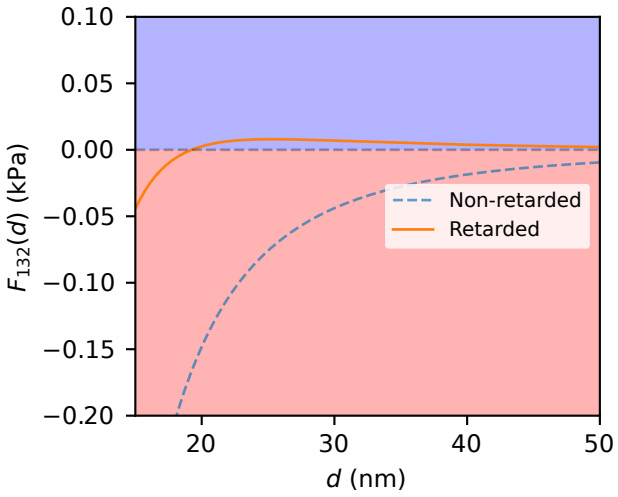

Figure 5: $F_{123}(d)$ (in kPa) as function of d.

Q2 Realistic Picture of Electric Double Layer

Q2.1 Limit analysis of Gouy-Chapman model

The differential capacitance of the Gouy-Chapman model is calculated as:

$$\begin{aligned} C_{\mathrm{EDL}}(\psi_{\mathrm{EDL}}) &= \frac{\mathrm{d}\sigma_{\mathrm{EDL}}}{\mathrm{d}\psi_{\mathrm{EDL}}} \\ &= -\frac{\varepsilon_0\varepsilon_{\mathrm{w}}\mathrm{d}(E_{\mathrm{EDL}})}{\mathrm{d}\psi_{\mathrm{EDL}}} \\ &= \sqrt{\frac{2z^2e^2\varepsilon_0\varepsilon_{\mathrm{w}}c_0}{k_{\mathrm{B}}T}}\cosh(\frac{ze\psi_{\mathrm{EDL}}}{2k_{\mathrm{B}}T}) \end{aligned} \tag{3}$$

The relative thickness of the EDL is calculated by using the capacitance formula for a parallel plate capacitor,

$$d_{\mathrm{EDL}} = \frac{\varepsilon_0\varepsilon}{C_{\mathrm{EDL}}} \tag{4}$$

With $\varepsilon = \varepsilon_{\mathrm{w}}$, $\Psi_0 = \Psi_{\mathrm{EDL}}$ and the other given values we reach $d_{\mathrm{EDL}} < 0.001\mathrm{nm}$, which makes physically no sense as such values are even smaller than Atom radii. We see that higher potentials for Ψ_0 result in even lower distances d_{EDL}, thus indicating a convergence of d_{EDL} to 0. This is highly inaccurate for a physical model but can be fixed by adding a finite distance dielectric layer as it is done for the Gouy-Chapman-Stern model with the Stern layer.

Q2.2 Boundary conditions of potential

Since there is no free (mobile) charges inside the Stern layer, the potential profile is **linear**. The boundary condition at the interface between the Stern layer and the EDL is the continuity of displacement field along the x-direction:

$$\begin{aligned} D_{\mathrm{S}}|_{x=d_{\mathrm{S}}} &= D_{\mathrm{EDL}}|_{x=d_{\mathrm{S}}} \\ \varepsilon_0\varepsilon_{\mathrm{S}}\frac{\mathrm{d}\psi}{\mathrm{d}x}\bigg|^{-}_{x=d_{\mathrm{S}}} &= \varepsilon_0\varepsilon_{\mathrm{w}}\frac{\mathrm{d}\psi}{\mathrm{d}x}\bigg|^{+}_{x=d_{\mathrm{S}}} \end{aligned} \tag{5}$$

By defining $\Delta\psi = \psi_0 - \psi_{\mathrm{EDL}}$ where ψ_{S} is the potential at the Stern layer / EDL interface, $\frac{\mathrm{d}\psi}{\mathrm{d}x}$ in the Stern layer is expressed as -$\Delta\psi/d_{\mathrm{S}}$. Combine this with the Gouy-Chapman model, we have the boundary condition as:

$$\varepsilon_{\mathrm{S}}\frac{\psi_0 - \psi_{\mathrm{EDL}}}{d_{\mathrm{S}}} = \varepsilon_{\mathrm{w}}\sqrt{\frac{8k_{\mathrm{B}}Tc_0}{\varepsilon_{\mathrm{r}}\varepsilon_0}}\sinh(\frac{ze\psi_{\mathrm{EDL}}}{2k_{\mathrm{B}}T}) \tag{6}$$

Q2.3 Potential profiles of GCS model, constant ψ_0

There are several ways to solve the potential profile. Although the Poisson-Boltzmann equation is second order ODE, within the Gouy-Chapman model you can simply solve it as a first-order ODE, since the relation between $\mathrm{d}\psi/\mathrm{d}x$ and ψ is explicitly known. Another approach is to use the analytical form of the Gouy-Chapman equation as shown in the Lecture notes:

$$\frac{\tanh(\frac{ze\psi}{4k_{\mathrm{B}}T})}{\tanh(\frac{ze\psi_0}{4k_{\mathrm{B}}T})} = \exp(-\kappa x) \tag{7}$$

The solution for the potential profiles in GC and GCS models can be seen in Figure 6. As can be seen, when c_0 increases, the potential profiles decays faster due to the shorter Debye length.

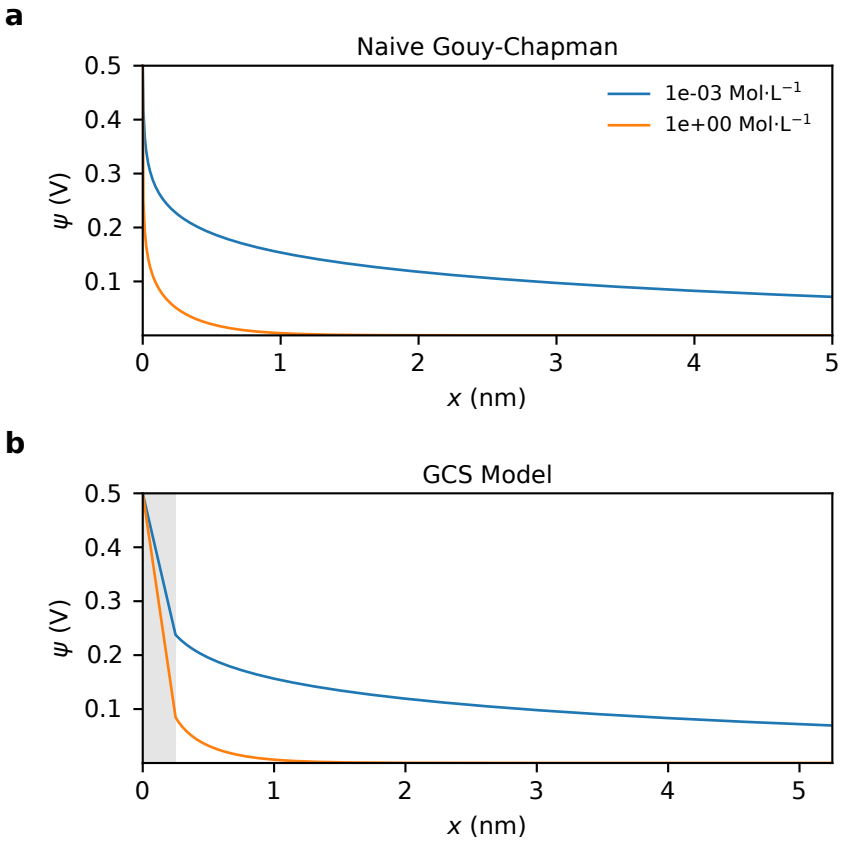

Figure 6: Potential profiles of different models with constant ψ_0. (a) naive Gouy-Chapman model with c_0 at 1 mM and 1 M. (b) GCS model with c_0 at 1 mM and 1 M. The region of the Stern layer is labeled in light grey.

On the other hand, we can see that the Stern layer reduces the interfacial potential ψ_{EDL}. For 1 mM salt ψ_{EDL} is about 0.23 V, while for 1 M salt ψ_{EDL} further decreases to about 80 mV, due to the larger electric field in the EDL.

Q2.4 Potential profiles of GCS model, constant σ_0

If we keep σ_0 at constant, since the capacitance of the EDL increases with more concentrated salt, the surface potential profile becomes lower for a concentrated salt. The behavior can be seen in Figure 7 when $\sigma_0 = 0.01$ C/m^2.

Q2.5 Differential capacitance

From Q2.1 we know that the differential capacitance of the Gouy-Chapman model is:

$$C_{\mathrm{EDL}}(\psi_{\mathrm{EDL}}) = \sqrt{\frac{2z^2e^2\varepsilon_0\varepsilon_{\mathrm{w}}c_0}{k_{\mathrm{B}}T}}\cosh\left(\frac{ze\psi_{\mathrm{EDL}}}{2k_{\mathrm{B}}T}\right) \tag{8}$$

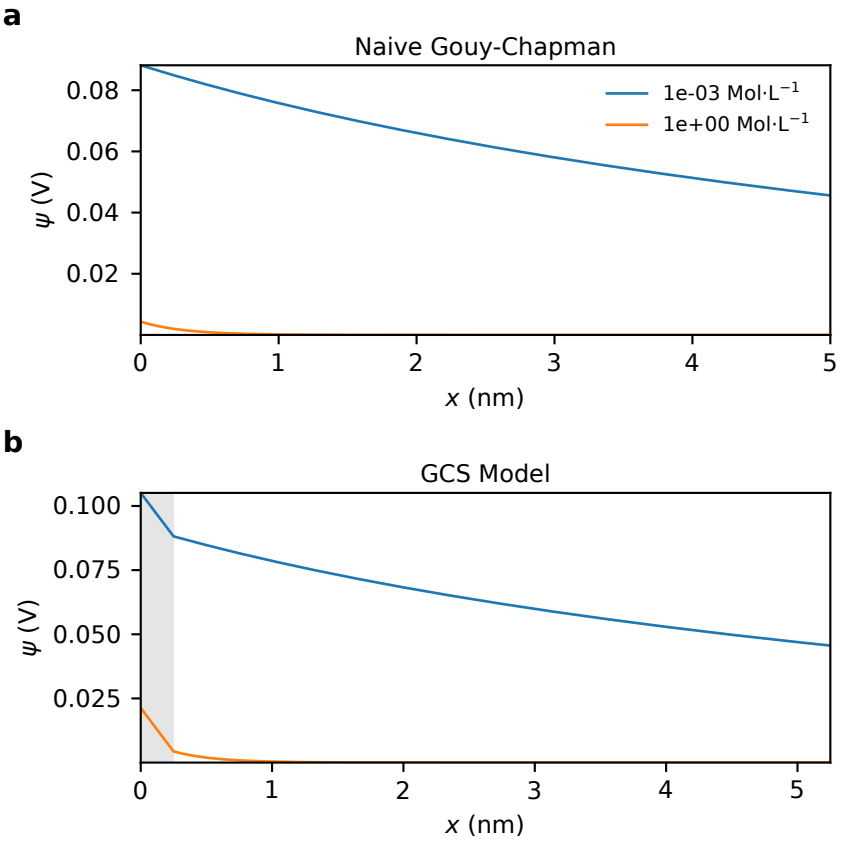

Figure 7: Potential profiles of different models with constant σ_0. (a) naive Gouy-Chapman model with c_0 at 1 mM and 1 M. (b) GCS model with c_0 at 1 mM and 1 M. The region of the Stern layer is labeled in light grey.

while the capacitance of the Stern layer is described by the parallel-plate capacitor:

$$C_S = \frac{\varepsilon_0 \varepsilon_S}{d_S} \tag{9}$$

The total differential capacitance of the system is calculated as capacitor-in-series:

$$C_{tot} = \left(\frac{1}{C_S} + \frac{1}{C_{EDL}(\psi_{EDL})}\right)^{-1} \tag{10}$$

the ψ_{EDL} has to be calculated using the boundary conditions in Q2.2. As shown in Figure 8, without the Stern layer, the capacitance increases dramatically with ψ_0, which makes such assumption unphysical. On the other hand, in the GCS model, the total capacitance is limited by the geometric capacitance of the Stern layer C_S, which is independent of the salt concentration.

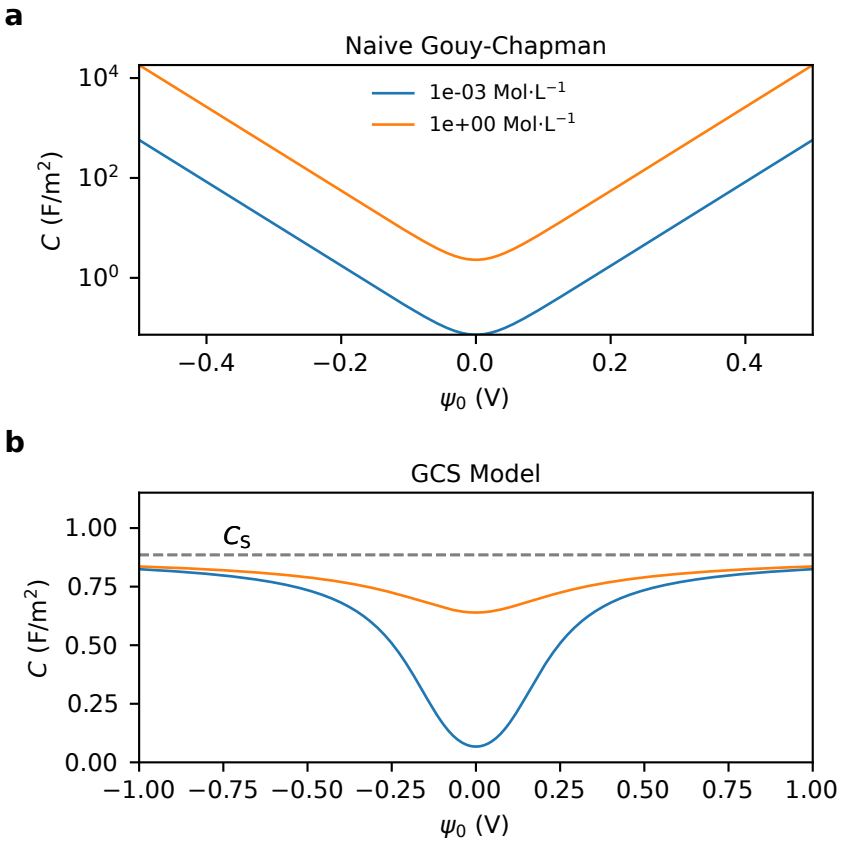

Figure 8: Total differential capacitance in (a) GC and (b) GCS models.

Q2.6 Direct comparison of GC and GCS model

In Figure 9 one can see the ratio between total differential capacitance of the GC and GCS model. We see that for the higher concentration both models don't coincide even for potentials smaller than 0.1V. For the lower concentration one can observe that both models differ by at least by approximately 1.08.

From this we can see that even for small potentials and concentration both models do not coincide for larger regions, thus meaning that in these cases both models are different. The coincidence of both models is highly dependent on the thickness of the Stern layer.

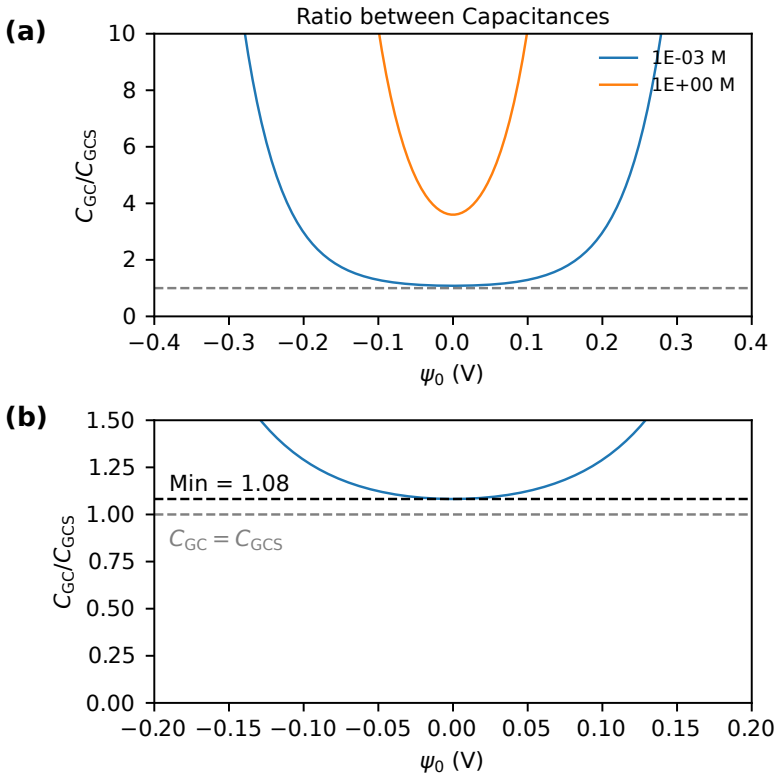

Figure 9: Ratio between total differential capacitance of GC and GCS model